CHAPTER 8

TECTONIC EVOLUTION

The similar paleostress fields are grouped together and two major, distinct deformation events – older D1 and younger D2 are defined that correspond to the regional tectonic events. The older D1 deformation event is further divided into two sub-groups – older D1o and younger D1y. Each sub-group should be considered as sub-type of the major deformation event owing to their similarity with the far-field stress conditions. The deformation phases defined here are multi-phase as the orientation of principal stress axes remains constant during the individual sub-type of major deformation events (Fossen et al., 2019). Furthermore, they cannot be considered as progressive in the sense that they are neither immediately preceding/following deformation phases nor showing gradual changes in stress orientations that may give rise to progressive deformation (Fossen et al., 2019). The deformation events are derived from the consistency among the deduced paleostress tensors from multiple paleostress analysis programmes. The age of faulted formations, attitude of principal stress axes, orientation of S_{Hmax} and S_{hmin}, stress regime index ($R^{/}$) and the governing stress regime are the parameters used to interpret the paleostress tensors belonging to the same deformation event. The paleostress map shown in Fig. 8.1 represents the orientation of S_{Hmax} and S_{hmin} for reverse faults and normal faults, respectively, derived for each of the studied sites. Since no absolute age information of timing of faulting are available, the reconstruction of sequence of deformation events is mainly based on the relative age information deduced in the field. In the VGKNFS, the major faults viz., NW striking VF and GUF are older and dislocate/terminate other NNE, NE, E oriented unnamed faults.

DERIVATION OF RELATIVE TIMING OF PALEOSTRESS STATE

Older D1 deformation event, Late Triassic to Late Cretaceous ~NW directed extension

The D1 event is characterized by paleostress tensors belonging to the extensional kinematics and is preferentially dominated by ~NW directed extension.

W, NW, NNW and NE striking S_{hmin} are observed in each sector. They belong to the NW striking major faults as well as NE oriented unnamed normal faults of local occurrence that terminate against the major faults. D1 event is most favorably represented by NE striking unnamed normal faults. They could not reactivate in later times due to their disorientation which is parallel to the ongoing compressional stress direction.

Following the data with normal fault kinematics in Sector 1, which mainly comprise of *(i)* NW directed extension represented by NE striking normal faults belonging to older D1o event (Fig. 8.2a), and *(ii)* WSW directed extension expressed by NNW striking GUF belonging to D1y event (Fig. 8.2b). These faults are formed under pure extensional stress regime with R' ranging 0.31-0.61 (Fig. 8.1). Around 63% of paleostress tensors represent normal faults kinematics in sector 1.

52% of the paleostress tensors represent extensional stress field in sector 2. Two distinct trends of S_{hmin} are observed: *(i)* NNW-NW oriented extension expressed by ENE and NE striking unnamed subsidiary faults respectively belonging to D1o event (Fig. 8.2a).

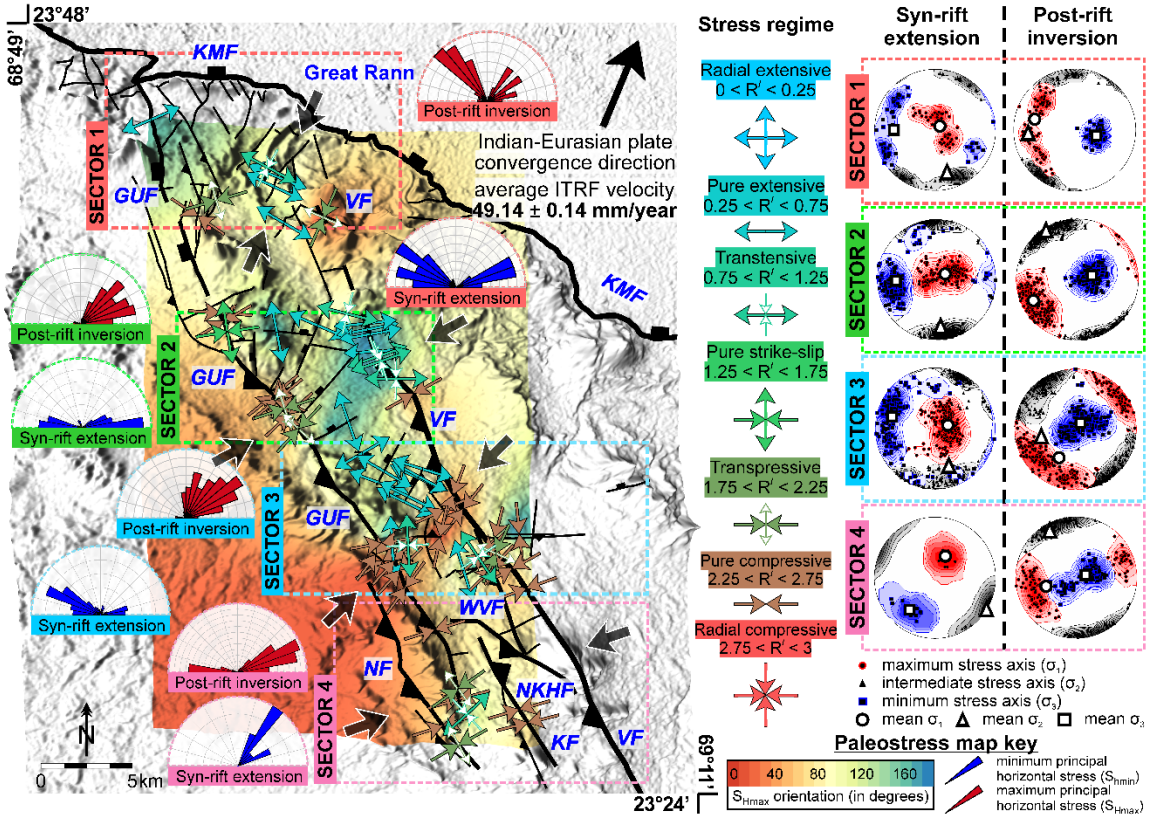

Fig. 8.1. Regional kinematics of the VGKNFS with reconstruction of the Late Mesozoic to Cenozoic paleostress orientations derived from fault-slip analysis. The biggest black inward-pointed double arrows (at the periphery of each sector) indicate the mean compressional directions derived for each of the four sectors. Inward-pointed and outward-pointed double arrows (within each sector): orientation of S_{Hmax} and S_{hmin} respectively. Colors given to arrows are according to the color scheme shown in vertical column of stress regime. Color scheme is based on the type of stress regime and stress index ($R^{/}$) (Delvaux et al., 1997). Rose plots show S_{Hmax} (red bars) and S_{hmin} (blue bars) orientation for each of the sector. On the right side of the map are sector-wise distribution of lower hemisphere, equal area projections for syn-rift extension and post-rift inversion phases representing principal stress axes (red circle: σ_1, black triangle: σ_2 and blue square: σ_3) population calculated for each site with kamb contours. The biggest circle, triangle and square in stereonet represent mean σ_1, σ_2 and σ_3 respectively. During syn-rift extension, sector 1: mean σ_1 at 052° ∠82°, mean σ_2 at 165° ∠25°, mean σ_3 at 270° ∠33°; sector 2: mean σ_1 at 056° ∠77°; mean σ_2 at 175° ∠20°, mean σ_3 at 267° ∠32°; sector 3: mean σ_1 at 086° ∠75°, mean σ_2 at 161° ∠29°, mean σ_3 at 283° ∠26°; sector 4: mean σ_1 at 026° ∠59°, mean σ_2 at 124° ∠03°, mean σ_3 at 216° ∠32°. During post-rift inversion, sector 1: mean σ_1 at 282° ∠34°, mean σ_2 at 264° ∠23°, mean σ_3 at 105° ∠60°; sector 2: mean σ_1 at 241° ∠22°, mean σ° at 326° ∠10°, mean σ_3 at 075° ∠70°; sector 3: mean σ_1 at 208° ∠45°, mean σ_2 at 254° ∠43°, mean σ_3 at 046° ∠80°; sector 4: mean σ_1 at 254° ∠48°, mean σ_2 at 330° ∠16°, mean σ_3 at 082° ∠77°. The average International Terrestrial Reference Frame (ITRF) velocity in the KRB is after Dumka et al. (2019). The colored overlay draped over shaded relief map represent S_{Hmax} orientation. Warm colors represent NNE–NE oriented S_{Hmax}.

(ii) ~W extension represented by NNW striking VF belonging to D1y event (Fig. 8.2b). Sector 2 constrains the VF showing normal and reverse slip-senses along its northern and southern segments, respectively. The northern segment is influenced by pure extensive to transtensive stress regime during D1y event and is characterized by ~W extension with $R^{/}$ ranging from 0.38-0.50 (Fig. 8.1). In the vicinity of the northern segment of VF, N-NNE striking, sub-vertical, systematic joints (site 100) exposed in Jhuran sandstone are characterized by ~W extension with $R^{/}$ of 0.99. The S_{hmin} strikes parallel to that of NNW striking VF with normal slip, testifying the fact that joints are generated during D1y event under transtensive stress regime. Thus, the systematic joints are related to far-field stresses and are not affected by local stress perturbations.

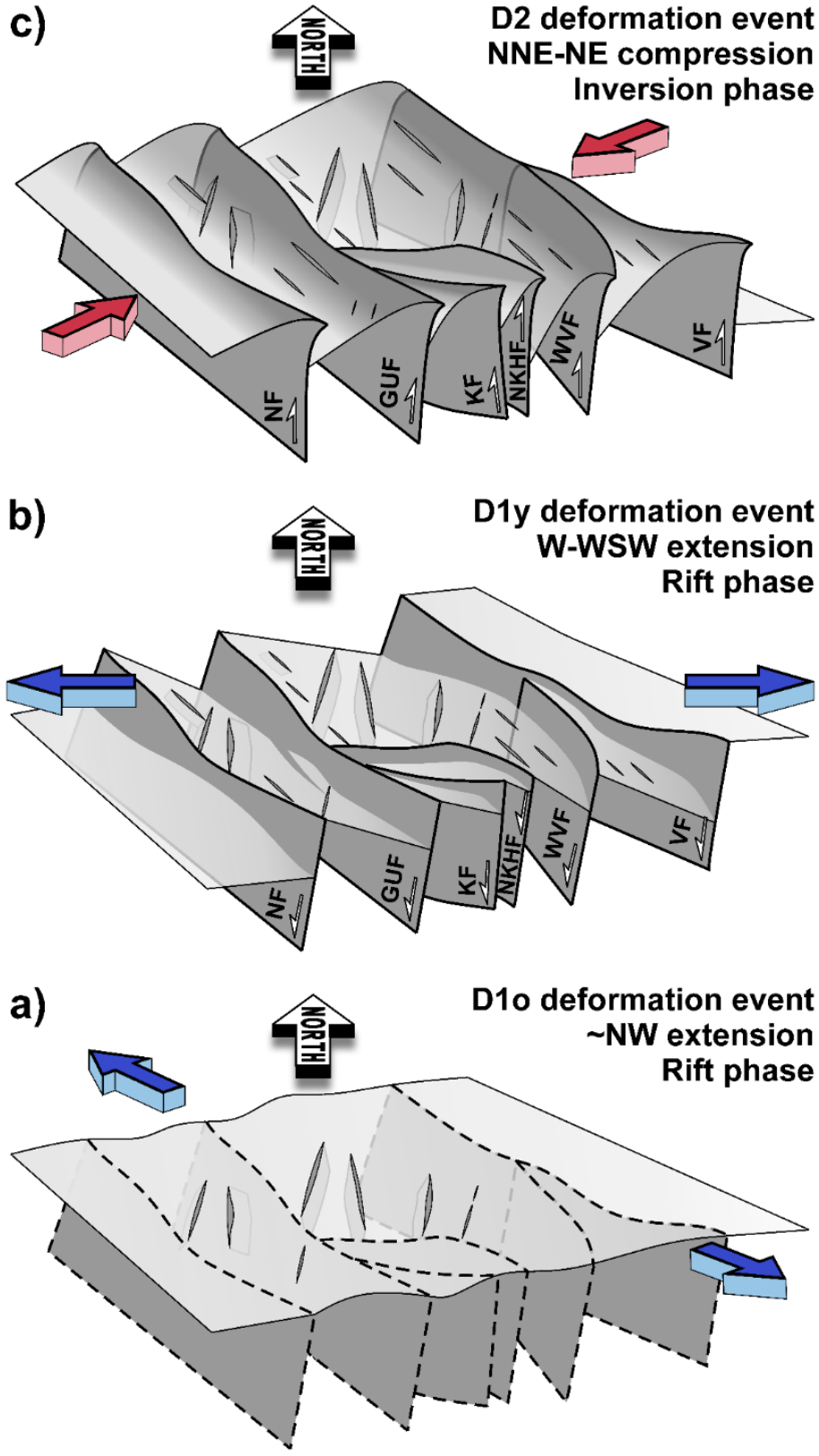
c)
NORTH
D2 deformation event
NNE-NE compression
Inversion phase
NF
GUF
KF
NKHF
WVF
VF
b)
NORTH
D1y deformation event
W-WSW extension
Rift phase
NF
GUF
KF
NKHF
WVF
VF
a)
NORTH
D1o deformation event
~NW extension
Rift phase

Fig. 8.2. Conceptual kinematic models to explain the effect of changing stress fields in the Vigodi-Gugriana-Khirasra-Netra Fault System (VGKNFS). Red, inward-pointed and blue, outward-pointed double arrows indicate the orientation of S_{Hmax} and S_{hmin} respectively. (a) D1o deformation event – Initiation of the rift phase of the KRB during Late Triassic. ~NW directed extension prevailed in the VGKNFS. Activation of NNE–NE striking discontinuous cross-faults as normal faults occurred. The NW striking pre-existing weak planes remained non-responsive. (b) D1y deformation event – continued rift phase of the KRB till Late Cretaceous. The extension direction swung from ~NW to W-WSW. Normal slip along the major NNW–NW striking faults occurred which eventually truncated the earlier activated NNE–NE striking cross-faults. (c) D2 deformation event – post-rift inversion phase of the KRB from Late Cretaceous till now. The build-up of NNE–NE directed compressional stress field that continues till now. The compressional reactivation of NNW–NW striking major faults occurred. NNE–NE striking cross-faults with normal slip continue to exist but remained non-responsive. The convex upward plunge of major faults in Fig. (c) indicate their upthrust geometry. Curved topography near major faults indicate narrow deformation zone. Note that the outcrop-scale structural complexities are ignored.

Sector 2 also exposes WNW and ENE striking unnamed, subsidiary faults with normal slip belonging to pure extensive stress regime of D1o event. They are characterized by NNW oriented S_{hmin} with R' of 0.49-0.64 (Fig. 8.1).

Sector 3 is characterized by *(i)* NE striking faults, *(ii)* E striking deformation band faults, *(iii)* NNE striking slipped deformation band, and *(iv)* NNW striking WVF. 45% of paleostress tensors represent extensional stress field in sector 3. NE striking subsidiary, unnamed faults show normal slip and are characterized by NW oriented S_{hmin} belonging to D1o event and are developed under pure extensive stress regime with R' ranging from 0.49-0.67 (Fig. 8.2a). Nearly E striking deformation band fault formed under pure extensive to transtensive stress regime is represented by ~N striking S_{hmin} with R' varying from 0.50-1.19. NNW striking WVF shows normal slip formed under pure extensive stress regime and is characterized by ~W striking S_{hmin} belonging to the D1y event with R' ranging from 0.48-0.63 (Fig. 8.2b). Thus, temporally, NW to W rotation of S_{hmin} came about in sector 3.

In sector 4, NW striking normal fault of local occurrence is represented by NE striking S_{hmin}, which has no role in the regional stress field. Except this one site, no other site in sector 4 shows signatures of extensional tectonics.

Relationship with the anticlockwise rotation of the Indian plate during Cretaceous

After the break-up of the Gondwanaland and India-Africa separation, drift movement of the Indian plate began with counter-clockwise rotation from mid-Jurassic time onward (Chatterjee et al., 2013). This induced transtensional movement in the KRB (Biswas, 2016). Although, strike-slip motion is not prominent and no structural signatures of trans-tension stress regime are observed on regional scale in the VGKNFS. None of the major faults in the VGKNFS display strike-slip motion. Sites with transpressional (e.g., site 6: GUF)/transtensional (e.g., site 23: VF) tectonics are due to local perturbations in the stress field and these do not mean that the VGKNFS experienced an overall transpressional/transtensional stress regimes. The striated faults denoting strike-slip motion are of sporadic occurrence. The dip-slip striations clearly seem to truncate strike-slip striations indicating that reverse movement is younger than strike-slip motion in the VGKNFS. On a regional context, above observations match well in the sense that the inversion of the KRB post-dates the drift of the Indian plate. Due to lack of sufficient number of fault-slip data with strike-slip motion (nt = 2), it is not included in the paleostress analysis. Therefore, no separate deformation event to strike-slip motion is assigned as the paleostress orientations are unknown.

Younger D2 deformation event, Late Cretaceous to Quaternary fault reactivation under NNE-NE compression

The younger D2 event characterized by the compressive stress regime is the predominant structural style in the VGKNFS since Late Cretaceous. It is represented by NNE-NE compression and is the most dominant and best-fitted stress regime to the present-day stress conditions in each of the sector of VGKNFS. The paleostress regimes in the study area involve three major compression directions – NNE, NE and E.

Reverse fault kinematics during D2 event is expressed by NW striking VF and NNE striking unnamed faults in sector 1. Around 37% of paleostress tensors belong to D2 event in sector 1. In its northernmost extremity, the VF reactivated under transpressive stress regime with N24° directed S_{Hmax} and R' of 2.03 belongs to the D2 event (Figs. 8.1, 8.2c). Another set of NE striking reverse faults reactivated under transpressive to pure compressive stress regime and show N74°-N124° oriented S_{Hmax}

with R' of 2.19 and 2.53 (Fig. 8.1). The ENE-ESE directed S_{Hmax} is not associated with the D2 event and it is due to the local perturbations in the stress field.

In sector 2, *(i)* the southern segment of VF and *(ii)* NW striking GUF with reverse slip are dominated by ~NE directed compression with R' ranging from 2.24-2.55 indicating the role of pure compressive stress regime (Fig. 8.2c). No unnamed cross-fault with NNE-E strike reactivated as reverse fault in sector 2. 48% of paleostress tensors represent compressional stress field in sector 2.

Sector 3 exposes NW striking VF and GUF, and NNW striking WVF that reactivated during D2 event under pure compressive stress regime with NNE-NE directed S_{Hmax} (Fig. 8.2c). Sector 4 exposes NNW striking GUF, and NW striking KF and NF that formed under pure compressive to transpressive stress regime with NE oriented S_{Hmax} (Fig. 8.2c). 55% and 88% of paleostress tensors represent D2 event in sectors 3 and 4 respectively.

Fault reactivation during basin inversion and its relation to Cenozoic Indian-Eurasian collision plate kinematics

The D2 event with NNE-NE oriented S_{Hmax} belonging to compressional stress regime (Late Cretaceous - till now) is expressed by NW striking major faults in the VGKNFS (Fig. 8.2c). The rifting of the KRB is followed by the rift inversion phase (tectonic cycle 2; as in Biswas, 2016). The NW striking major faults in the VGKNFS dip at high-angle but not sub-vertical. So, there is no question that they will get locked in inversion tectonics. As the far-field compressive stresses are at right angles, the normal faults formed during rifting, reactivated as high-angle reverse faults and certainly, there is not any possibility that they resolved into strike-slip motion. Therefore, the VGKNFS cannot be interpreted as the riedel shear system bounded by the KMF and KHF.

The compressional stress field with NNE-NE oriented S_{Hmax} is generated by: *(i)* Collision of the Indian plate with the southern margin of Eurasia at the convergent margin in Late Paleocene-Eocene, which generated N-NE verging back-thrust at the collision front (Gowd et al., 1992). This vergence of back thrusting happened in the Himalaya and it is now well-documented and discussed. The post-Indian-Eurasian plate collisional far-field compressive stress field is continuing till date causing neotectonic

movements in the KRB (Biswas, 2016; Shaikh et al., 2019). *(ii)* The spreading Carlsberg ridge at the divergent margin in the Indian Ocean exerts horizontal ridge push force resulting from the excess thermal elevation of young oceanic lithosphere (Eagles and Wibisono, 2013).It generated intra-plate stresses ENE towards the KRB and contributed to the Indian plate motion (Biswas, 2016).Along the western Indian plate margin, the Chaman fault system with left-lateral strike-slip motion does not contribute to build-up of intra-plate stresses in the KRB.

IS THE VIGODI-GUGRIANA-KHRIASRA-NETRA FAULT SYSTEM (VGKNFS) REALLY SENSITIVE TO THE FAR-FIELD STRESS?

Chi-Square Statistic

A statistical approach was adopted to address the question mentioned above. The goodness-of-fit test was performed to analyze the chi-square statistic. Goodness-of-fit calculation is a statistical hypothesis that provides a way to assess how well the obtained S_{Hmax} orientations through paleostress analysis fit with the ongoing NNE directed compressional stress field. Mean S_{Hmax} orientation derived for major and unnamed cross-faults through paleostress analysis was taken as the input parameter. The limitations of this analysis are:

(i) faults with reverse slip are included in the analysis while the major and unnamed faults with normal slip are excluded,

(ii) the test requires a sufficient sample size of S_{Hmax} orientation to establish chi-square approximation to be valid and therefore, goodness-of-fit calculation could not be performed for the WVF (number of observations $i = 2$), KF ($i = 2$), NF ($i = 2$) and slipped deformation band ($i = 1$).

The results are represented in the form of a chart as shown in Fig. 8.3. The test was performed using the following equation:

$$\chi^2 = \frac{\{(S_{Hmax})_{mean} - (S_{Hmax})_{predicted}\}^2}{\{(S_{Hmax})_{std.\ dev.}\}^2}$$

Here, χ^2 = chi squared value calculated as the goodness-of-fit function, $(S_{Hmax})_{mean}$ = mean orientation of S_{Hmax} calculated through paleostress analysis in the present study, $(S_{Hmax})_{predicted}$ = NNE oriented S_{Hmax} in the contemporary compressional

stress field, $(S_{Hmax})_{std.\ dev.}$ = standard deviation of a range of orientations of S_{Hmax} computed through paleostress analysis in the present study.

The mean S_{Hmax} orientation of VF, WVF, GUF, KF, NF and unnamed cross-faults were calculated for each of the sectors and plotted on the graph. The uncertainty or variability in the population of calculated S_{Hmax} orientations was estimated by calculating standard error for the respective fault in each of the four sectors. The calculated standard error has been graphically represented in the form of an error bar (Fig. 8.3). The red horizontal line depicts the mean S_{Hmax} of N23° E derived by Gowd and Rao (1992) using BO-, FSM- and hydro-fracturing data. The mean S_{Hmax} orientations not falling in the N0°-90° E interval were excluded (indicated by black box area in Fig. 8.3).

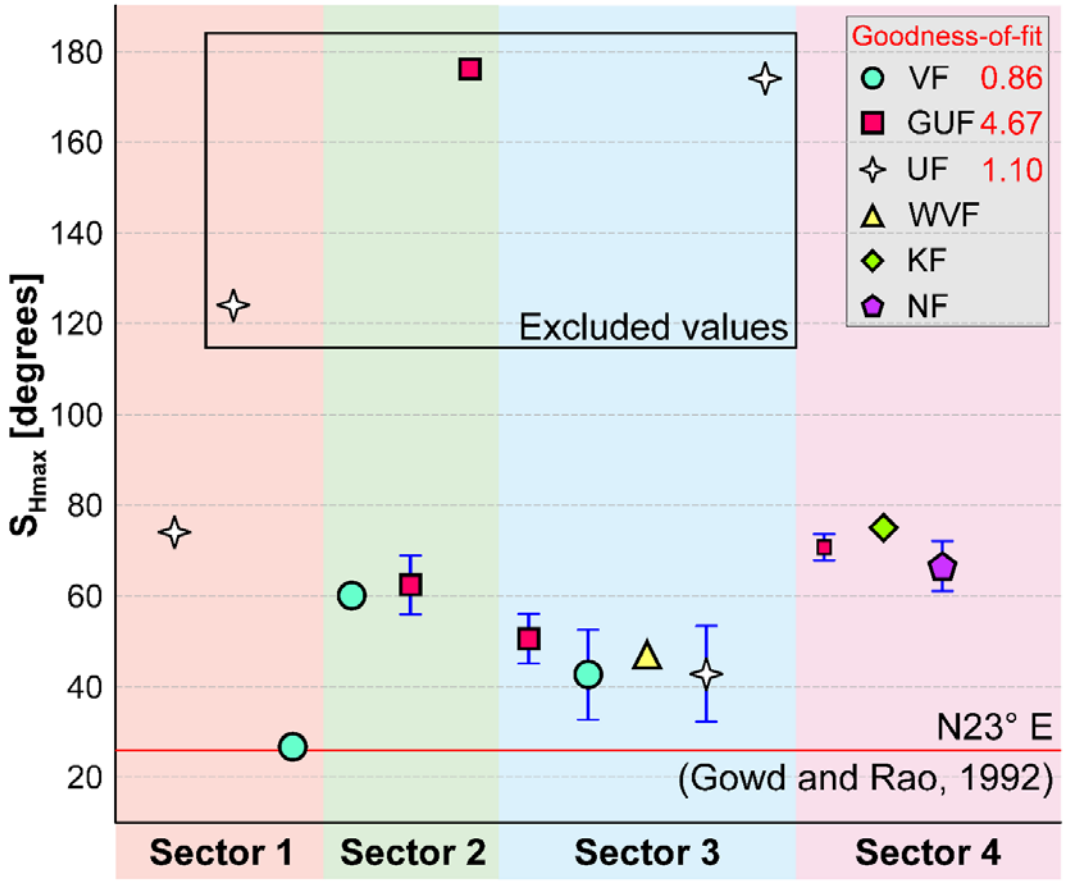

Fig. 8.3. Plot showing sector-wise distribution of the mean S_{Hmax} orientation corresponding to major faults and unnamed cross-faults with reverse slip. The results of chi-square statistic are also shown.

In the scenario of VGKNFS,

(i) $\chi^2 \leq 1$; represented by the observed values fall within the data uncertainty. The measured S_{Hmax} orientations to have a "good" fit to the regional contemporary NNE oriented compressional stress field. The VF ($\chi^2 = 0.86$) shows close fit with the ongoing NNE oriented compression stress field. It also points to the likelihood of fault reactivation, although, other important parameters e.g., the observed fault geometry combined with estimated stress orientation and magnitude should also be taken into account.

(ii) $\chi^2 > 1$; represented by any observed values that fall outside the data uncertainty interval. The calculated S_{Hmax} orientations to have a "poor" fit to the contemporary NNE oriented compressional stress field. The GUF ($\chi^2 = 4.67$) shows the highest discrepancy or skewness between the calculated S_{Hmax} and the ongoing NNE oriented S_{Hmax}. Since the goodness-of-fit value for unnamed cross-faults ($\chi^2 = 1.10$) is very close to 1, it can be considered that the derived S_{Hmax} orientations for the unnamed cross-faults with reverse slip fairly match with the contemporary NNE oriented compressional stress field.

REGIONS ILLUSTRATING MAXIMUM HORIZONTAL COMPRESSION IN VGKNFS AND THEIR RELEVANCE TO THE INDIAN PLATE MOTION

The paleostress map depicted in Fig. 8.1 highlights the density of S_{Hmax} orientations. The potential zones of stress accumulation are highlighted by warm colors. The mean S_{Hmax} orientations in the compressional stress regime, obtained for the major faults in each of the sectors, can be correlated with the convergence (/absolute plate motion) direction of the Indian plate. The convergence direction is nearly orthogonal to NE boundary of the Indian plate (Lacombe, 2012). The absolute plate motion direction of the Indian plate is ~N40° E (Singh and Mandal, 2020). From sector 1 to 4, the angle of divergence are 16°, 22°, 06° and 30° respectively. Thus, statistically, it can be inferred that sector 3showing highest uplift in the VGKNFS, exhibits less obliquity to the Indian plate convergence direction than those in the other sectors. In the intra-plate regions characterized by compressional stress regime, the orientation of S_{Hmax} is generally parallel to the direction of absolution plate motion (Zoback et al., 1989). Thus, in the

present study, *(i)* low divergence-angle of S_{Hmax} to the Indian plate convergence direction and, *(ii)* spatial homogeneity of the *in situ* stress field, in both, reverse and normal faulting stress regime suggest that the far-field stresses dominate over the near-field stress condition to govern the intra-plate stress distribution in the KRB.

CONGRUENCE WITH THE PRESENT-DAY STRESS STATE

It would be interesting to compare the paleostress field inferred from the present work with the contemporary stress field in the KRB. Till date, no studies have been carried out to infer present-day stress state in the study area. However, myriad work has been done in the eastern part of the KRB that can be accounted for comparison with paleostress conditions inferred in the study area at the western part of the KRB. Several studies related to inversion of earthquake FMS (Mandal, 2013 and references therein), GPS derived surface displacement measurements (Dumka et al., 2019; Gahalaut et al., 2019 and references therein), InSAR data (Chandrasekhar et al., 2009 and references therein) and offshore BO (Sen et al., 2019 and references therein) provide extensive constraints on the recent kinematics of the active KRB. For example, Richardson et al. (1979) computed ~N oriented S_{Hmax}. Gowd and Rao (1992) estimated mean S_{Hmax} to be N23° E for the mid-continental stress province of India (central and northern India) using BO(~1-3.5 km depth), FMS(~15-33 km depth) and hydro-fracturing(~150-590 m depth) data. The World Stress Map (WSM) compiled compressional faulting regime with N02°-05° E and N148°-178° E striking S_{Hmax}, and strike-slip faulting regime with N152°-178° E and N14° E striking S_{Hmax} using FMS; and NE oriented S_{Hmax} using BO in the eastern part of the KRB, ~120-150 km east of the present study area (Heidbach et al., 2016; 2018). Sen et al. (2019) interpreted S_{Hmax} to be N10°-N20° E using BO in the offshore Kachchh-Saurashtra region. Mallik et al. (2008) carried out Electromagnetic Radiation (EMR) investigations to infer the S_{Hmax} to be N60° E ± 10°. Patra and Saha (2019) also reported N-S compression from eastern Himalaya. The paleostress analysis results belonging to D2 event are consistent with the inferred present-day kinematics in the sense that the NW striking major, reactivated reverse faults in the VGKNFS show NNE-NE striking S_{Hmax}.